Accepted Manuscript

A TiO_2 Nanosheet-g-C_3N_4 composite photoelectrochemical enzyme biosensor excitable by visible irradiation

Peipei Liu, Xiaohe Huo, Yunfei Tang, Jun Xu, Xiaoqiang Liu, K.Y.Wong Danny

PII: S0003-2670(17)30749-3

DOI: 10.1016/j.aca.2017.06.043

Reference: ACA 235291

To appear in: *Analytica Chimica Acta*

Received Date: 10 February 2017

Revised Date: 27 June 2017

Accepted Date: 28 June 2017

Please cite this article as: P. Liu, X. Huo, Y. Tang, J. Xu, X. Liu, K.Y. Danny Wong, A TiO_2 Nanosheet-g-C_3N_4 composite photoelectrochemical enzyme biosensor excitable by visible irradiation, *Analytica Chimica Acta* (2017), doi: 10.1016/j.aca.2017.06.043.

A TiO_2 Nanosheet-g-C_3N_4 Composite Photoelectrochemical Enzyme Biosensor Excitable by Visible Irradiation

Peipei Liu[a], Xiaohe Huo[a], Yunfei Tang[a], Jun Xu[a], Xiaoqiang Liu[a*], and Danny K.Y.Wong[b**]

[a] Institute of Environmental and Analytical Sciences, College of Chemistry and Chemical Engineering, Henan University, Kaifeng, Henan Province, 475004, P.R.China

[b] Department of Chemistry and Biomolecular Sciences, Macquarie University, Sydney, NSW 2109, Australia

[*] Corresponding author: Tel: +86 13781157777; E-mail:13781157777@163.com

[**] Corresponding author: Tel: +61 2-9850-8300; E-mail: Danny.Wong@mq.edu.au

ABSTRACT:

In this work, g-C_3N_4 and TiO_2 nanosheets were synergistically employed as a novel composite for developing a scaffold of a photoelectrochemical enzyme biosensor. In this way, we have improved the poor visible light excitation of TiO_2 and retarded the photo-generated charge recombination on g-C_3N_4 to achieve an enhanced response at the photoelectrochemical biosensor, compared to that generated by the corresponding biosensors consisting of each individual component. Using glucose oxidase as a model enzyme, the biosensor was demonstrated to show strong visible light activity towards the enzyme mediated glucose oxidation. We have also observed a 350% enhanced photocurrent compared to that at a g-C_3N_4 based ITO electrode. In addition, the high specific surface area and excellent biocompatibility of TiO_2 nanosheets have also positively contributed to the performance of the photoelectrochemical enzyme biosensor with a 0.05 – 16 mM linear range and a 0.01 mM glucose detection limit**.**

Keywords:
g-C_3N_4; TiO_2nanosheets; photoelectrochemical enzyme biosensor; glucose oxidase.

1. Introduction

In recent years, photoelectrochemical PEC biosensors have emerged as a new promising analytical tool in biological and biochemical assays due to their synergistic advantages from electroanalytical and photocatalytic methods [1]. The performance of these PEC biosensors is strongly dependent on the electrochemical and photochemical properties of the materials immobilised on the sensor surface [2]. As a consequence, different photoactive semi-conductor materials such as TiO_2, CdS, SnO_2, ZnO and ZnS have been prepared for PEC sensor developments in order to exploit their biocompatibility, moderate conductivity and strong photocatalytic properties [3, 4]. However, these photoactive semi-conductors have also displayed inherent disadvantages including photocorrosion, low visible-light absorption and unsatisfactory conductivity, which have restrained their applications to PEC sensors [5]. Several reports [6-8] have previously demonstrated that composting the semi-conductors with other materials to be an effective way to improve their performance and minimise the shortcomings. For example, graphene-TiO_2 nanohybrids exhibited a nearly 5-time enhanced photocurrent relative to TiO_2 nanocrystals alone under visible light [9]. A PEC sensor based on graphene-TiO_2 nanohybrid was developed for the ultrasensitive determination of nicotinamide adenine dinucleotide and a linear dynamic range between 0.01 and 2000 μM with a detection limit of 0.003 μM was obtained.

In the form of a network of two-dimensional conjugated s-triazine rings, polymeric graphite-like carbon nitride g-C_3N_4 exhibited a small band gap of ~2.7 eV, making visible light excitation of g-C_3N_4 possible [10, 11]. Accordingly, g-C_3N_4 was reportedly used as a visible light driven metal-free photocatalyst in PEC applications such as production of H_2 and O_2 from water spitting [12]. The combination of TiO_2 nanoparticles and g-C_3N_4 has been frequently used in photocatalysis as a visible light catalyst because of their ideally matched energy levels [13-15]. These energy levels in the composite are then expected to narrow the gap of TiO_2, making visible light excitation possible and reducing the recombination of photo-generated charges of g-C_3N_4, which would otherwise impede the photochemical and PEC applications of g-C_3N_4. In addition, the low specific surface area

of g-C_3N_4 resulted by their bulk volume could be enhanced by composting with other materials with high surface area.

There have hitherto been very few applications of g-C_3N_4-TiO_2 to PEC sensor developments, most likely because of their bulky volume, relatively low specific surface area and poor conductivity of TiO_2 nanoparticles. Fortunately, the emerging two-dimensional TiO_2 nanomaterials such as nanosheets, nanofilms and nanofibres have demonstrated unique features including high specific surface area, fast charge transfer and improved PEC properties relative to nanoparticles [16]. For example, Yan *et al*. [17] have constructed a PEC biosensing platform by assembling CdSe quantum dots and DNA on a TiO_2 film modified electrode, which sensitively responded to *o*-aminophenol under visible light irradiation. The single-crystalline two-dimensional TiO_2 film significantly increased the lifespan of the photo-generated charges and improved the PEC activity because of their large surface area and strong electron transportation capability provided by the two-dimensional structure [18, 19].

In the present work, a new composite between g-C_3N_4 and two-dimensional TiO_2 nanosheets was synthesised, as illustrated in Scheme 1. Another novelty of our work is the application of the g-C_3N_4-TiO_2 composite as an effective material for constructing a PEC biosensor by entrapping the model enzyme, glucose oxidase (GOx). Two-dimensional TiO_2 nanosheets with a high specific surface area were exploited to accommodate a substantial load of biomolecules, while their biocompatibility is expected to aid in retaining the catalytic activity of the enzyme on glucose at the electrode. Additionally, g-C_3N_4 was strategically used to minimise the band gap of the composite so that the PEC sensor would be excitable by visible irradiation to avoid possible deactivation of GOx by UV light. In this way, the glucose biosensor was demonstrated to exhibit high sensitivity and reliable detection characteristics for glucose in the absence of mediators under visible irradiation.

2. Experimental

2.1 Material and reagents

In our work, 1, 3, 5-triazine-2, 4, 6-triamine was purchased from BASF Chemical Co. Ltd Tianjin, China. Titanium(IV) isopropoxide (≥97%) was purchased from Alfa Aesar Chemical Co. Ltd Tianjin, China and diethylenetriamine (99% purity) was acquired from J&K Scientific Ltd Beijing, China. GOx and Nafion were purchased from Sigma Aldrich, USA. Glucose was obtained from Tianjing Chemical Reagent Company. All chemicals were of analytical grade and used without further purification. A 0.1 M phosphate buffered saline (PBS; pH 7.4) was used as a supporting electrolyte throughout the experiments. All solutions were prepared in MilliQ water.

2.2. Instrumentation

Electrochemical and PEC measurements were carried out on a CHI630D electrochemical workstation Shanghai CH Instruments, China. A Xe lamp (CEL-HXUV 300; Beijing AULTT, China) equipped with a visible light monochromators was used as the photo-excitation source. Indium tin oxide ITO electrodes were acquired from Wuhan Lattice Solar Energy Technology. Ltd., China. Electrochemical impedance spectroscopy was conducted using an IM6ex electrochemical workstation (Zahner, Germany). The morphology of nanomaterials was characterised by transmission electron microscopy (Tecnai G2 20, USA). The chemical composition of samples was determined using an X-ray photoelectron spectrometer (ESCALAB 250Xi, USA) with a monochromated Al Kα source *hv* 1486.6 eV, 150 W power and a 500 μm beam spot. The X-ray photoelectron spectra were calibrated based on the C1s peak 284.8 eV and analysed using the XPSPEAK41 software (Department of Chemistry, The Chinese University of Hong Kong, China). Crystallographic information of samples was collected by an X-ray diffractometer (Bruker D8 Advance, Germany) with a Cu Kα radiation λ=1.5406 nm, while infrared spectra were obtained using a Fourier transform infrared spectrometer (12 Nicolet 170, USA). Diffuse reflectance spectra of samples were monitored by a UV–visible spectrophotometer (UV-2600, Kyoto, Japan).

2.3. Preparation of g-C_3N_4, g-C_3N_4-TiO_2 composite and TiO_2 nanosheets

As described previously [20], g-C_3N_4 sheets were synthesised by pyrolysis of tripolycyanamide powder. Specifically, 5.0 g of tripolycyanamide powder in a closed ceramic crucible was heated at 550°C in air for 4 h at a rate of 5°C min^{-1} in a muffle furnace. After cooling to room temperature in air, the yellow g-C_3N_4 was pulverised into a fine powder and collected for use without any further treatment.

The g-C_3N_4-TiO_2 composite was synthesised using a previously reported method [21] that we have then modified. The procedure is illustrated in Scheme 1. Briefly, 40 mg of g-C_3N_4 was dispersed in 40 mL isopropyl alcohol by sonication for 30 min, prior to adding 0.03 mL diethylenetriamine. After gentle stirring for 5 min, 1.8 mL of titanium(IV) isopropoxide was added with stirring. The solution was then transferred to a 50 mL Teflon-lined stainless steel autoclave that was kept in an oven at 200°C for 12 h. The autoclave was allowed to cool down to room temperature. The light yellow precipitate of g-C_3N_4-TiO_2 composite was collected by centrifugation, washed thoroughly with ethanol, and dried at 60°C overnight. TiO_2 nanosheets were prepared as previously reported [22]. In this procedure, 40 mg of multi-walled carbon nanotubes and 0.03 mL diethylenetriamine were dispersed in 40 mL isopropyl alcohol by sonication before 1.8 mL of titanium(IV) isopropoxide was added with stirring. The mixed solution was then transferred to a Teflon-lined stainless steel autoclave kept in an oven at 200°C for 12 h. After cooling down to room temperature, the precipitate was collected by centrifugation, washed thoroughly with ethanol, and dried at 60°C overnight. To obtain TiO_2 nanosheets, the as-prepared composite was calcinated at 500°C for 2 h to remove excess carbon nanotubes from the composite.

2.4. Electrochemical Measurements

Electrochemical measurements were carried out at a CHI630D electrochemical workstation with a three-electrode system consisting of a modified ITO working electrode, a platinum wire auxiliary electrode, and a Ag|AgCl (3.0 M KCl) reference electrode. All electrochemical impedance spectroscopic experiments were performed in 0.1 M KCl containing 5 mM $[FeCN_6]^{3-}$ and 5 mM $[FeCN_6]^{4-}$ over a frequency range from 100 kHz to

0.1 Hz. A constant DC potential of 0.23 V superimposed by an AC potential of 5 mV was applied and the resultant AC current was measured to calculate the impedance at each frequency. All results obtained were presented as Nyquist (imaginary impedance (*Z"*) versus real impedance (*Z'*)) plots, which were then fitted using a SIM software associated with the IM6ex impedance analyser (Zahner, Germany).

2.5. Preparation of a PEC biosensor

In preparing a GOx|g-C_3N_4-TiO_2|ITO biosensor, an ITO electrode 2.5 cm length × 1.0 cm width was successively rinsed for 30 min with acetone, ethanol and ultrapure water under ultrasonication, and dried at room temperature. Meanwhile, 20 mg of g-C_3N_4-TiO_2 nanomaterials was dispersed in 300 µL of aqueous GOx solution (2 mg mL^{-1}) containing 50 µL Nafion (5% w/w) and the mixture was agitated in a thermostat oscillator at 4°C for 4 h. Finally, 20 µL of this mixture was applied on a clean ITO glass of 0.25 cm^2 area and dried at 4°C for 8 h. For comparison, a g-C_3N_4|ITO and a g-C_3N_4-TiO_2|ITO were also fabricated using the same procedure without GOx.

2.6. PEC assay procedure

PEC experiments were performed using a homemade PEC system using a 300 W Xe lamp (PLS-300/3000UV) as the irradiation source with an intensity of 150 W cm^{-2} between 400 and 780 nm. PEC experiments were carried out using a CHI630D electrochemical workstation with a three-electrode system consisting of an ITO working electrode, a platinum wire auxiliary electrode, and an Ag|AgCl (3.0 M KCl) reference electrode. In all experiments, a pH 7.4 PBS was used as a supporting electrolyte. A potential of 0.2 V was applied to the ITO electrode in each PEC experiment, and the photocurrent was recorded as the excitation light was switched on and off.

3. Results and discussion

The present work is aimed at developing a PEC enzyme biosensor excitable by visible irradiation for the detection of glucose. In developing this biosensor, we have initially prepared a g-C_3N_4-TiO_2 composite that was used to entrap GOx before being secured by Nafion on an ITO electrode. In the following sections, we have systematically

characterised each component of the scaffold before it was evaluated for optimal analytical biosensor performance.

3.1. Characterisation of TiO_2 nanosheets, g-C_3N_4 and g-C_3N_4-TiO_2 composites

In this work, g-C_3N_4 was initially prepared by pyrolysis of tripolycyanamide powder. Then TiO_2 nanosheets were solvothermally formed on top of g-C_3N_4 using titanium(IV) isopropoxide as a precursor. The crystal structure of TiO_2 nanosheets, g-C_3N_4 and a g-C_3N_4-TiO_2 composite was investigated by X-ray diffraction and the spectra obtained are correspondingly displayed as trace (i), (ii) and (iii) in Figure 1(a). In trace (i), the pattern of TiO_2 nanosheets exhibits several typical peaks of anatase TiO_2 at 25.3º, 37.9º, 48.0º, 54.1º, 55.1, 62.7º, 68.8º, 70.2º, and 75.0º, which are correspondingly attributed to the (1 0 1), (0 0 4), (2 0 0), (1 0 5), (2 1 1), (2 0 4), (1 1 6), (2 2 0), and (2 1 5) crystal faces, after comparing these results to those reported obtained in the development of nanostructured S-doped TiO_2 thin films [23]. In contrast, in trace (ii), only two peaks at 13.1° and 27.4° were observed. By comparing to a previous report in which a TiO_2 nanoparticle-g-C_3N_4 composite was prepared for photocatalysis [24], the peak at 13.1^o is assigned to the 100 plane of tri-s-triazine units in g-C_3N_4, while the peak at 27.4^o is attributed to 002 crystal face of the interlayer stacking of conjugated aromatic segments. Notably, the g-C_3N_4-TiO_2 sample presents the diffraction peaks of both g-C_3N_4 and TiO_2 in trace (iii). According to Li *et al*. [25], who prepared Ti^{3+} self-doped TiO_2/g-C_3N_4 heterojunctions for photocatalytic applications, the diffraction peaks at 25.4^o, 38.1^o, 48.3^o, 54.2^o and 62.7^o are correspondingly assigned to the (101), (004), (200), (211) and (204) crystal faces of anatase TiO_2. However, the peak of g-C_3N_4 at ~13.1^o is absent in trace (ii), while only a small peak at 27.4^o is observable, most likely due to the low percentage composition of g-C_3N_4 in the composite. Therefore, these X-ray diffraction results generally support the formation of a composite between g-C_3N_4 and TiO_2.

The chemical structures of TiO_2 nanosheets, g-C_3N_4 and the g-C_3N_4-TiO_2 composite were next analysed by Fourier transform infrared spectroscopy. As shown in trace (i) of Figure 1(b), TiO_2 nanosheets have shown a strong adsorption band between 400 and 800 cm^{-1} attributing to the Ti-O stretching and Ti-O-Ti bridging vibration, and two distinct

absorption bands centered at ~3430 $cm^{-1}$and 1640 cm^{-1}, respectively, which are assigned to the hydroxy stretching and bending vibrations on their surface [26]. The spectrum of g-C_3N_4, in trace (ii) of Figure 1(b) displays a sharp absorption peak at 810 cm^{-1}, which was assigned to the breathing mode of tri-s-triazine units of g-C_3N_4 after comparing to the results obtained by Dong *et al*. [27] in the preparation of the visible light photocatalyst of g-C_3N_4. We use this to infer the presence of 1,3,5-triazine-2,4,6-triamine in g-C_3N_4. The formation of a dimer of 1,3,5-triazine-2,4,6-triamine will then yield aromatic secondary and tertiary amines [28], accounting for the peaks at 1247, 1323, 1411 and 1460 cm^{-1}. Furthermore, the broad peaks in the range of 3100-3500 cm^{-1} region can be ascribed to the usual N-H stretching from the residual amino groups and the -OH band from adsorbed H_2O molecules. More importantly, all the absorption peaks of g-C_3N_4 are readily observable in the spectrum of g-C_3N_4-TiO_2 composite shown in trace (iii), in addition to the strong absorption bands between 500 $cm^{-1}$and 800 cm^{-1} assigned to the bonds of Ti-O and Ti-O-Ti [26]. In this way, trace (iii) has confirmed that g-C_3N_4 in the composite did not decompose during the hydrothermal process and the composite material was successfully synthesised.

The optical property of the nanomaterials was characterised by UV-visible diffuse reflectance spectroscopy. Trace (i), (ii) and (iii) in Figure 1(c) are the corresponding UV-visible absorption spectra of g-C_3N_4, g-C_3N_4-TiO_2 and TiO_2 nanosheets alone. According to trace (i) and (ii), g-C_3N_4 absorbed light at a wavelength up to 460 nm, while TiO_2 only exhibited strong absorption below 400 nm trace (iii), supporting a smaller band gap of g-C_3N_4 than that of TiO_2. Therefore, these results indicate that the presence of g-C_3N_4 has narrowed the band gap of the composite, which contributed to the shift of the absorption edge to the visible light.

The morphology of TiO_2 and the g-C_3N_4-TiO_2 composite was studied by transmission electron microscopy and scanning electron microscopy. As shown in Figure 2(a), the transmission electron micrograph of g-C_3N_4 presents a semitransparent sheet structure with dimensions of several micrometers. The g-C_3N_4 sheets resemble wrinkled silk veil and provide an enlarged platform for the immobilisation of other nanomaterials and biomolecules. Figure 2(b) shows the transmission electron micrograph of g-C_3N_4-TiO_2

247 composite, in which TiO_2 nanomaterials appear to be darker than g-C_3N_4 despite that both
248 materials are semitransparent. Scanning electron micrographs of the composite have also
249 been acquired to verify the formation of TiO_2 nanosheets on g-C_3N_4. Figure 2(c) displays
250 the existence of laminar structures on a coarse surface. The magnified image of these
251 laminar structures in Figure 2(d) appears to show that the TiO_2 nanosheets on g-C_3N_4
252 sheets and the TiO_2 nanosheets are approximately a few hundred nanometres in dimension,
253 which is smaller than that of the g-C_3N_4 sheets. We have also noted that the TiO_2
254 nanosheets could no longer be separated from the C_3N_4 nanosheet after ultrasonication,
255 suggesting a very strong interaction between the TiO_2 and C_3N_4 nanosheets. Previously,
256 Fan *et al*. and Xu *et al*. [29, 30] have reported that heterojunctions were formed between
257 TiO_2 and g-C_3N_4, which would aid in the transfer of photogenerated electrons at our PEC
258 sensor.
259
260 X-ray photoelectron spectroscopic measurements were carried out to obtain information on
261 the chemical state and surface composition of the composite. The survey spectrum in
262 Figure 3(a) indicates the presence of Ti, O, C and N in the g-C_3N_4-TiO_2 composite, as
263 supported by the features described below. The high resolution C1s spectrum in Figure
264 3(b) displays three peaks centred at 284.6, 286.2 and 288.2 eV. Based on Singh *et al*.'s
265 [31] work concerning gold nanoparticles deposited on C_3N_4 for the gas and liquid phase
266 oxidation of CO, the peak at 284.6 eV may be attributed to contaminated carbon and
267 surface carbon, while the 286.2eV and 288.2 eV peaks arose from C=O and N=C-N_2
268 groups of g-C_3N_4, respectively. The X-ray photoelectron spectrum of N1s in Figure 3(c)
269 was deconvoluted using the XPSPEAK41 software into three peaks at binding energy of
270 398.5, 399.5 and 401.3 eV, in agreement with those reported by Li *et al*. [32]. The N1s at
271 binding energy of 398.5 eV was assigned to sp^2-hybridised nitrogen C-N=C, as described
272 by Zhang *et al*. [33], who used g-C_3N_4 for efficient sunlight-driven photocatalytic hydrogen
273 production. The remaining two peaks at 399.5 and 401.3 eV were attributed to tertiary
274 nitrogen N-C_3 and amino functional groups with a hydrogen atom -NH_2 or =NH,
275 respectively [34]. Figure 3(d) shows the Ti2p spectrum of g-C_3N_4-TiO_2 composite.
276 According to Liu *et al*. [35], who investigated a TiO_2−SiO_2−Ag nanocomposite
277 photocatalyst by utilising lysozyme as both an inducing agent of TiO_2 and a reducing agent

of Ag^{+}, the $Ti2p_{3/2}$ peak at 458.6 and the $Ti2p_{1/2}$ peak at 464.3 eV were ascribed to Ti^{4+} species in the form of TiO_2 clusters. Meanwhile, Figure 3(e) displays two O1s peaks at 530.0 and 531.2eV that were ascribed to oxygen in TiO_2 and surface hydroxyls(-OH), respectively, after comparing to Boonprakob *et al*'s work on photocatalytic degradation of methylene blue using a g-C_3N_4/TiO_2 film [36]. Based on atomic ratio of 16.14% C, 10.61% N, 24.32% Ti and 48.93% O in the X-ray photoelectron spectrum in Figure 3(a), the mass ratio between TiO_2 and g-C_3N_4 was estimated to be 5.9, indicating a relatively low percentage of g-C_3N_4 in the composite. These X-ray photoelectron spectroscopic results, in conjunction with the microscopic, X-ray diffraction, and Fourier transform infrared results, clearly revealed the formation of a binary composite material with strong binding between g-C_3N_4 and TiO_2, rather than a simple physical mixture of two separate g-C_3N_4 and TiO_2 phases.

3.2. Electrochemical and PEC characterisation of GOx biosensor

Electrochemical impedance spectroscopy has been demonstrated to be a powerful tool for the study of material conductivity and interfacial properties of modified electrodes. In this work, electrochemical impedance spectroscopy of 5.0 mM $[FeCN_6]^{3-}$ and 5.0 mM $[FeCN_6]^{4-}$ was used to investigate the stepwise interfacial assembly of the immunosensor in 0.1 M KCl. Figure 4(a) displays a series of Nyquist plots obtained at the half-wave potential of 230 mV estimated from the cyclic voltammogram shown in the inset. These plots exhibited a semicircle in the high frequency region and a linear feature in the low frequency region. An equivalent circuit also presented as an inset in Figure 4(a) consisting of a double layer capacitor C_{dl} in a parallel arrangement with both an electron transfer resistance R_{et} and a Warburg diffusion impedance W, all of which are in a series arrangement with a solution resistance Rs, was used to generate theoretical Nyquist plots that would fit with the experimental Nyquist plots. Based on the optimal values of the circuit elements tabulated in Figure 4(a), the diameter of a semicircle corresponding to R_{et} of the $[FeCN_6]^{3-}$ and $[FeCN_6]^{4-}$ couple at the modified electrode surface was estimated. As expected, the bare ITO electrode trace (i) exhibits the smallest R_{et} of 32 Ω among all these plots, demonstrating the highest conductivity. More importantly, R_{et} of 315 Ω at the g-C_3N_4|ITO trace (ii) is substantially larger than that of 71 Ω at the g-C_3N_4-TiO_2|ITO trace

(iii), indicating that the electrical conductivity of g-C_3N_4-TiO_2 has been improved with respect to that of g-C_3N_4 alone. As displayed in Scheme 2, both the conduction band and the valence band of g-C_3N_4 are at a higher energy level than those of a TiO_2 nanosheet, which will benefit the transfer of photo-generated charges and minimise their recombination. Consequently, the free charges in the composite will be significantly increased after the formation of the composite, leading to an enhanced conductivity. The improved conductivity of g-C_3N_4-TiO_2 will benefit the performance of a g-C_3N_4-TiO_2 based PEC sensor. Trace (iv) shows the Nyquist plot obtained after immobilising GOx on the g-C_3N_4-TiO_2|ITO. An R_{et} of 164 Ω is 131% larger than that of g-C_3N_4-TiO_2|ITO trace (iii), as the nanomaterial composite and biomolecules immobilised on the electrode surface were now acting as barrier layers for the electron transfer of $[FeCN_6]^{3-}$ and $[FeCN_6]^{4-}$, giving rise to an increased R_{et}. These results indicate that GOx was successfully immobilised on the electrode surface.

We have next examined the biocatalytical activity response of the GOx|g-C_3N_4-TiO_2|ITO biosensor to glucose. Previously, the cyclic voltammogram of free flavin adenine dinucleotide FAD known to be the electroactive site of GOx at a graphene modified electrode in nitrogen-saturated PBS showed a reversible redox couple with a formal potential at ~0.45 V versus a Ag|AgCl reference electrode 3 M KCl, pH 7 [37]. These voltammetric peaks were therefore assigned to the direct electron transfer of free FAD, as opposed to FAD still entrapped within GOx [38]. Similarly, a pair of reversible voltametric peaks between -0.4 and -0.5 V at a GOx-carbon nanotube modified electrode was used to indicate that FAD has extruded out of GOx by carbon nanotubes immobilised on the electrode [39]. This would therefore be expected to cause a permanent loss of GOx bioactivity towards glucose. In our work, we have initially obtained a featureless voltammogram between 0 and -0.7 V, as displayed in trace (i) of Figure 4(b), at a GOx|g-C_3N_4-TiO_2|ITO biosensor in nitrogen-saturated PBS. The absence of any redox peaks in the cyclic voltammogram would therefore support that FAD was being retained within GOx during the experiment.

When the experiment was repeated in air-saturated PBS, the obtained cyclic voltammogram, denoted by trace (ii) in Figure 4(b), shows a large cathodic peak current at ~-0.42 V. According to Liang *et al*. [38], in such an experiment, GOx(FAD) reacts with its substrate, glucose, to produce GOx($FADH_2$) represented by Equation 1 below, which is then oxidised back to GOx(FAD) in the presence of O_2 (Equation 2)

$$GOx(FAD) + glucose \rightarrow GOx(FADH_2) + gluconolactone \quad \text{Equation 1}$$

$$GOx(FADH_2) + O_2 \rightarrow GOx(FAD) + H_2O_2 \quad \text{Equation 2}$$

Therefore, the cathodic peak at ~-0.42 V in trace (ii) is attributed to the electrochemical reduction of O_2. The O_2 reduction current decreased with increasing glucose concentration in the air-saturated solution trace (iii) to trace (v) owing to the consumption of the dissolved O_2 by GOx($FADH_2$) produced in the enzyme catalytic glucose oxidation (Equation 1). This result demonstrates that GOx immobilised on the electrode retained their enzyme activity in the presence of O_2, which is a required criterion for the PEC application.

3.3 Optimisation of the PEC biosensor

In our work, we have studied the effect of Nafion concentration on photocurrent response of the GOx|g-C_3N_4-TiO_2|ITO sensor in 0.1 M PBS containing 1 mM glucose by applying a bias potential of 0.2 V. As illustrated in Figure 4(c), the photocurrent increased with Nafion concentration up to 0.7% w/w and then slightly decreased. Most probably, the initial increase has arisen from the capability of the Nafion layer in minimising the leakage of GOx from electrode surface. However, a retarded transport of redox mediators by a dense Nafion film on the electrode, when >0.7% w/w Nafion was used, has resulted in diminished current. Similarly, the effect of mass ratio between GOx and the composite on the PEC response of the sensor was also optimised in 0.1 M PBS containing 1 mM glucose. Figure 4(d) shows that the photocurrent response was enhanced rapidly with increasing GOx concentration from 0.05 to 3% w/w and then plateaued off. In these experiments, excess GOx would cause steric hindrance and therefore impede the electrons transfer.

3.4. PEC evaluation of the PEC biosensor

The photocurrent generated at g-C_3N_4|ITO, g-C_3N_4-TiO_2|ITO, GOx|g-C_3N_4-TiO_2|ITO and GOx|g-C_3N_4-TiO_2|ITO in the presence of glucose in PBS was measured to investigate the PEC behaviour of the nano-material modified ITO. In all these experiments, we have adopted a constant voltage of 0.2 V from a previous report involving the detection of lactate at a PEC biosensor in 0.1 M PBS [40]. Irrespective of analytes, this potential was demonstrated to effectively separate the photogenerated holes and electrons, and minimise electrooxidation of possible interfering species at higher potential. Figure 5(a) shows a plot of PEC response at the different modified electrodes versus time as the visible irradiation was switched on and off over several cycles. Due the poor visible light excitation, TiO_2 nanosheet|ITO trace (i) has exhibited the lowest photocurrent among all the modified ITO electrodes. A ~3-fold larger photocurrent was obtained at g-C_3N_4|ITO trace (ii) due to the easy recombination between the photo-generated electrons and holes on pure g-C_3N_4. When g-C_3N_4-TiO_2|ITO was irradiated by visible light, the photo-generated electrons became excited and they were transferred from the conduction band of g-C_3N_4 to that of TiO_2 and therefore avoided their recombination with the holes. Accordingly, the photocurrent at g-C_3N_4-TiO_2|ITO trace (iv) has increased ~3.5 times than that at g-C_3N_4|ITO. As illustrated in Scheme 2, GOx oxidises glucose to gluconic acid, while O_2 is simultaneously reduced to H_2O_2. Under visible irradiation, the photo-generated electrons from g-C_3N_4 will be injected into the conduction band of TiO_2, and then attracted to the positive ITO electrode. At the same time, the photo-generated holes of TiO_2 will move to the valence band of g-C_3N_4, and then consumed by H_2O_2. Both the conduction band and the valence band of g-C_3N_4 are at a higher energy level than those of a TiO_2 nanosheet, which will benefit the transfer of photo-generated charges and minimise their recombination. Upon immobilising GOx on the electrode, the photocurrent at GOx|g-C_3N_4-TiO_2|ITO trace (iii) is ~26% smaller than that at g-C_3N_4-TiO_2|ITO trace (iv). More importantly, the photocurrent at GOx|g-C_3N_4-TiO_2|ITO has increased by 66.4% trace (v) after 1 mM glucose was added to the 50 mL PBS in the cell. In the experiment, GOx catalysed the reduction of O_2 to H_2O_2, which then acted as an electron donor, as illustrated in Scheme 2. The consumption of H_2O_2 by photogenerated holes has impeded the recombination of photo-generated charges and therefore increased the photocurrent [41]. Notably, in Figure 5(a), the photocurrent took a longer time to reach stability after GOx

was immobilised on the biosensor platform. This is most likely because the separated photo-irradiated charges were still able to quickly generate a stable photocurrent in the absence of biomolecules. Moreover, a considerable quantity of the GOx molecules (2 mg mL^{-1} aqueous solution) immobilised on the modified ITO electrode would impede the transfer of photo-generated holes and electrons on the nano-composite. This would therefore prolong the time for the photocurrent to reach stability. However, the analytical performance would not be affected by keeping the photo-irradiated time constant during experiment.

Time-dependent photocurrent measurement at GOx|g-C_3N_4-TiO_2|ITO was conducted at several representative glucose concentrations from 0.05 to 16.0 mM. As displayed in Figure 5(b), the photocurrent remained highly stable at each glucose concentration and rapidly responded to the repeated on-off cycles of irradiation, confirming the excellent PEC performance of the sensor. The photocurrent in Figure 5(b) is also observed to increase with glucose concentration, as shown by a background current corrected ΔI calibration plot in Figure 5(c). The calibration plot can be represented by the following relationship from 0.05 to 16 mM with a statistically significant correlation coefficient of 0.995 N=6 at the 95% confidence level:

$$\Delta I / \mu A = 7.711 \pm 1.014 + 16.67 \pm 2.318 \log_{10} [\text{glucose}] / \mu A\ mM^{-1}$$

where the uncertainty indicates the 95% confidence interval. In addition, the result of a Wald-Wolfowitz runs test confirmed a random pattern of the residuals, further supporting a linear calibration relation. Accordingly, a sensitivity of 16.67 μA cm^{-2} mM^{-1} and a detection limit at a signal-to-noise ratio of 3 of 0.01 mM were estimated for the GOx|g-C_3N_4-TiO_2|ITO biosensor. The analytical performance of the PEC biosensor is compared to that of several other glucose sensors tabulated in Table 1, and our biosensor has shown comparable analytical performance in terms of sensitivity, detection limit and linear range. The performance of the GOx|g-C_3N_4-TiO_2|ITO biosensor is attributed to the special properties of g-C_3N_4-TiO_2 including strong visible light absorption and low charge recombination. The composite also provided a biocompatible micro-environment for retaining GOx bioactivity and facilitated strong capability in promoting direct electron transfer of GOx at the electrode surface.

The repeatability at GOx|g-C_3N_4-TiO_2|ITO electrodes was examined by six successive determinations of 0.4 mM glucose at single electrodes. A relative standard deviation RSD was estimated to be 3.8%, demonstrating good repeatability of the PEC biosensors. Six PEC biosensors were prepared independently using the same protocol to examine the fabrication reproducibility of the biosensors. They were used to detect 0.4 mM glucose under the same experimental conditions. The reproducibility with an RSD of 4.4% was obtained. To assess the stability, GOx|g-C_3N_4-TiO_2|ITO electrodes were stored at 4℃ and then used to daily measure the current response of 1 mM glucose. The PEC sensor retained 90.5% of its original current response over a storage period of 2 weeks, indicating that the enzyme bioactivity was maintained in the g-C_3N_4-TiO_2 composite.

The PEC biosensor was also used to detect glucose in human serum samples. The serum samples were obtained from The Laboratory Centre of our local hospital and were initially spectrophometrically analysed at the hospital using a Mindray BS-380 Model biochemical analyser set at a wavelength of 285 nm. Following a 50-fold dilution of each serum sample in 0.1 M PBS, the glucose concentration in the sample was measured by the GOx|g-C_3N_4-TiO_2|ITO biosensor. The results reported by the hospital and those obtained using the PEC biosensor are tabulated in Table 2. Using paired t-test, there was no significant difference found between the two sets of results at the 95% confidence level. In addition, a recovery between 96.0% and 103% was estimated in the results obtained at the PEC biosensor. Therefore, the GOx|g-C_3N_4-TiO_2|ITO PEC biosensor displays a high potential for practical analysis of glucose in clinical samples.

Possible interference on the detection of glucose was evaluated by the PEC detection of 1 mM glucose in pH 7.4 PBS containing individually 0.1 mM ascorbic acid, uric acid, dopamine, fructose, lactose and sucrose, as shown in Figure 5(d). Based on a photocurrent change of 3.7–5.6% for ascorbic acid, uric acid and dopamine, less than 1.7% for fructose and lactose, the reagents used did not appear to have a significant interfering effect on glucose detection at the PEC biosensor. The results suggested an excellent selectivity of the glucose biosensor toward glucose.

3. Conclusions

In summary, a novel nanocomposite of g-C_3N_4-TiO_2 was formed by growing TiO_2 on g-C_3N_4 nanosheets. This nanocomposite was then successfully applied to develop a PEC glucose biosensor. The formation of the composite was confirmed by microscopic, spectroscopic and electrochemical techniques. The subsequent PEC evaluation shows a ~350% enhanced PEC efficiency at the g-C_3N_4-TiO_2 hybrid structure with respect to both g-C_3N_4 nanosheets alone and TiO_2 alone. The GOx|g-C_3N_4-TiO_2| ITO sensor exhibits satisfactory performance in the detection of glucose, indicating the great application potential of the prepared composite in the PEC biosensors. In addition, the PEC sensing experiments were performed under low bias voltages and relied on visible light as an excitation source, which are advantageous characters for the development of safe, convenient, fast and easy-to-use glucose detection devices in future.

Acknowledgments

This work was financially supported by National Natural Science Foundation of China (No. U1504215，21576071), International Science and Technology Cooperative Project funded by The Department of Science and Technology of Henan Province (172102410042) and the Scientific Research Foundation for the 46th Batch Returned Overseas Chinese Scholars, State Education Ministry.

Table 1. Analytical performance of several relevant GOx PEC biosensors.

GOx PEC Biosensors	Dynamic range / mM	Detection limit / mM	References
TiO_2/CdSe@CdS/GOx	1-10	N/A	[42]
GOx/Ag_2S/SnO_2/ITO	0.1-12.2	0.032	[43]
α-Fe_2O_3 cubes/ITO	0.2-2.0	0.015	[44]
GOx/CdTe/ITO	0.1-11	0.04	[45]
Graphene-CdS/ITO	0.1-4.0	0.007	[46]
BiOCl-G NHS[c]/ITO	0.5-10	0.22	[47]
GOx|g-C_3N_4-TiO_2|ITO	0.05-16	0.01	This work

[a] inverse opal photonic crystals; [b]F doped SnO_2 electrode; [c] bismuth oxychloride-graphene nanohybrid sheets.

;

Table 2. Determination of glucose in human serum samples.

Samples	Spectrometry / mM	Detected at Biosensor / mM	Recovery	RSD N = 6
1	4.45	4.59	103%	4.3%
2	4.52	4.34	96.0%	3.9%
3	6.16	6.28	102%	4.8%

References

[1] X. Zhang, Y. Zhao, S. Li, S. Zhang, Photoelectrochemical biosensor for detection of adenosine triphosphate in the extracts of cancer cells, Chem. Commun., 46 (2010) 9173-9175.

[2] W.-W. Zhao, Z.-Y. Ma, D.-Y. Yan, J.-J. Xu, H.-Y. Chen, In situ enzymatic ascorbic acid production as electron donor for CdS quantum dots equipped TiO_2 nanotubes: A general and efficient approach for new photoelectrochemical immunoassay, Anal. Chem., 84 (2012) 10518-10521.

[3] W. Tu, Y. Dong, J. Lei, H. Ju, Low-potential photoelectrochemical biosensing using porphyrin-functionalized TiO_2 nanoparticles, Anal. Chem., 82 (2010) 8711-8716.

[4] J. Tang, B. Kong, Y. Wang, M. Xu, Y. Wang, H. Wu, G. Zheng, Photoelectrochemical detection of glutathione by IrO_2–Hemin–TiO_2 nanowire arrays, Nano Lett., 13 (2013) 5350-5354.

[5] S. Klosek, D. Raftery, Visible light driven v-doped TiO_2 photocatalyst and its photooxidation of ethanol, J. Phys. Chem. B, 105 (2001) 2815-2819.

[6] S. Cheng, W. Fu, H. Yang, L. Zhang, J. Ma, H. Zhao, M. Sun, L. Yang, Photoelectrochemical Performance of Multiple Semiconductors (CdS/CdSe/ZnS) Cosensitized TiO2 Photoelectrodes, J. Phys. Chem. C, 116 (2012) 2615-2621.

[7] W.-W. Zhao, S. Shan, Z.-Y. Ma, L.-N. Wan, J.-J. Xu, H.-Y. Chen, Acetylcholine esterase antibodies on BiOI nanoflakes/TiO2 nanoparticles electrode: A case of application for general photoelectrochemical enzymatic analysis, Anal. Chem., 85 (2013) 11686-11690.

[8] G.-C. Fan, H. Zhu, D. Du, J.-R. Zhang, J.-J. Zhu, Y. Lin, Enhanced photoelectrochemical immunosensing platform based on CdSeTe@CdS:Mn core–shell quantum dots-sensitized TiO_2 amplified by CuS nanocrystals conjugated signal antibodies, Anal. Chem., 88 (2016) 3392-3399.

[9] K. Wang, J. Wu, Q. Liu, Y. Jin, J. Yan, J. Cai, Ultrasensitive photoelectrochemical sensing of nicotinamide adenine dinucleotide based on graphene-TiO_2 nanohybrids under visible irradiation, Anal. Chim. Acta, 745 (2012) 131-136.

[10] A. Thomas, A. Fischer, F. Goettmann, M. Antonietti, J.-O. Muller, R. Schlogl, J.M. Carlsson, Graphitic carbon nitride materials: variation of structure and morphology and their use as metal-free catalysts, J. Mater. Chem., 18 (2008) 4893-4908.

[11] H. Yin, Y. Zhou, B. Li, X. Li, Z. Yang, S. Ai, X. Zhang, Photoelectrochemical immunosensor for microRNA detection based on gold nanoparticles-functionalized g-C_3N_4 and anti-DNA:RNA antibody, Sens. Actuators, B, 222 (2016) 1119-1126.

[12] X. Wang, K. Maeda, A. Thomas, K. Takanabe, G. Xin, J.M. Carlsson, K. Domen, M. Antonietti, A metal-free polymeric photocatalyst for hydrogen production from water under visible light, Nat Mater, 8 (2009) 76-80.

[13] X.-j. Wang, W.-y. Yang, F.-t. Li, Y.-b. Xue, R.-h. Liu, Y.-j. Hao, In situ microwave-assisted synthesis of porous N-TiO_2/g-C_3N_4 heterojunctions with enhanced visible-light photocatalytic properties, Ind. Eng. Chem. Res., 52 (2013) 17140-17150.

[14] S. Zhao, S. Chen, H. Yu, X. Quan, G-C_3N_4/TiO_2 hybrid photocatalyst with wide absorption wavelength range and effective photogenerated charge separation, Sep. Purif. Technol., 99 (2012) 50-54.

[15] J. Lei, Y. Chen, F. Shen, L. Wang, Y. Liu, J. Zhang, Surface modification of TiO_2 with g-C_3N_4 for enhanced UV and visible photocatalytic activity, J. Alloys Compd., 631 (2015) 328-334.

[16] Y. Wang, Y.-Y. Zhang, J. Tang, H. Wu, M. Xu, Z. Peng, X.-G. Gong, G. Zheng, Simultaneous etching and doping of TiO_2 nanowire arrays for enhanced photoelectrochemical performance, ACS Nano, 7 (2013) 9375-9383.

[17] K. Yan, R. Wang, J. Zhang, A photoelectrochemical biosensor for o-aminophenol based on assembling of CdSe and DNA on TiO_2 film electrode, Biosens. Bioelectron., 53 (2014) 301-304.

[18] P. Maggie, S. Karthik, K.V. Oomman, K.M. Gopal, A.G. Craig, Application of highly-ordered TiO_2 nanotube-arrays in heterojunction dye-sensitized solar cells, J. Phys. D: Appl. Phys., 39 (2006) 2498.

[19] C.A. Grimes, Synthesis and application of highly ordered arrays of TiO_2 nanotubes, J. Mater. Chem., 17 (2007) 1451-1457.

[20] S. Ye, L.-G. Qiu, Y.-P. Yuan, Y.-J. Zhu, J. Xia, J.-F. Zhu, Facile fabrication of magnetically separable graphitic carbon nitride photocatalysts with enhanced photocatalytic activity under visible light, J. Mater. Chem. A, 1 (2013) 3008-3015.

[21] X. Liu, R. Yan, J. Zhu, X. Huo, X. Wang, Development of a photoelectrochemical lactic dehydrogenase biosensor using multi-wall carbon nanotube -TiO_2 nanoparticle composite as coenzyme regeneration tool, Electrochim. Acta, 173 (2015) 260-267.

[22] P. Si, S. Ding, J. Yuan, X.W. Lou, D.-H. Kim, Hierarchically structured one-dimensional TiO_2 for protein immobilization, direct electrochemistry, and mediator-free glucose sensing, ACS Nano, 5 (2011) 7617-7626.

[23] S.Y. Arman, H. Omidvar, S.H. Tabaian, M. Sajjadnejad, S. Fouladvand, S. Afshar, Evaluation of nanostructured S-doped TiO_2 thin films and their photoelectrochemical application as photoanode for corrosion protection of 304 stainless steel, Surf. Coat. Technol., 251 (2014) 162-169.

[24] F. Dong, Z. Zhao, T. Xiong, Z. Ni, W. Zhang, Y. Sun, W.-K. Ho, In situ construction of g-C_3N_4/g-C_3N_4 metal-free heterojunction for enhanced visible-light photocatalysis, ACS Appl. Mater. Interfaces, 5 (2013) 11392-11401.

[25] K. Li, S. Gao, Q. Wang, H. Xu, Z. Wang, B. Huang, Y. Dai, J. Lu, In-situ-reduced synthesis of Ti^{3+} self-doped TiO_2/g-C_3N_4 heterojunctions with high photocatalytic performance under LED light irradiation, ACS Appl. Mater. Interfaces, 7 (2015) 9023-9030.

[26] H. Yan, H. Yang, TiO_2–g-C_3N_4 composite materials for photocatalytic H_2 evolution under visible light irradiation, J. Alloys Compd., 509 (2011) L26-L29.

[27] F. Dong, L. Wu, Y. Sun, M. Fu, Z. Wu, S.C. Lee, Efficient synthesis of polymeric g-C_3N_4 layered

materials as novel efficient visible light driven photocatalysts, J. Mater. Chem., 21 (2011) 15171-15174.

[28] I. Papailias, T. Giannakopoulou, N. Todorova, D. Demotikali, T. Vaimakis, C. Trapalis, Effect of processing temperature on structure and photocatalytic properties of g-C_3N_4, Appl. Surf. Sci., 358, Part A (2015) 278-286.

[29] M. Xu, L. Han, S. Dong, Facile fabrication of highly efficient g-C_3N_4/Ag_2O heterostructured photocatalysts with enhanced visible-light photocatalytic activity, ACS Appl. Mater. Interfaces, 5 (2013) 12533-12540.

[30] D. Fan, C. Guo, H. Ma, D. Zhao, Y. Li, D. Wu, Q. Wei, Facile fabrication of an aptasensor for thrombin based on graphitic carbon nitride/TiO_2 with high visible-light photoelectrochemical activity, Biosens. Bioelectron., 75 (2016) 116-122.

[31] J.A. Singh, S.H. Overbury, N.J. Dudney, M. Li, G.M. Veith, Gold nanoparticles supported on carbon nitride: influence of surface hydroxyls on low temperature carbon monoxide oxidation, ACS Catal., 2 (2012) 1138-1146.

[32] Y. Li, J. Zhang, Q. Wang, Y. Jin, D. Huang, Q. Cui, G. Zou, Nitrogen-rich carbon nitride hollow vessels: synthesis, characterization, and their properties, J. Phys. Chem. B, 114 (2010) 9429-9434.

[33] Y. Zhang, J. Liu, G. Wu, W. Chen, Porous graphitic carbon nitride synthesized via direct polymerization of urea for efficient sunlight-driven photocatalytic hydrogen production, Nanoscale, 4 (2012) 5300-5303.

[34] S.C. Yan, Z.S. Li, Z.G. Zou, Photodegradation performance of g-C_3N_4 fabricated by directly heating melamine, Langmuir, 25 (2009) 10397-10401.

[35] C. Liu, D. Yang, Y. Jiao, Y. Tian, Y. Wang, Z. Jiang, Biomimetic synthesis of TiO_2–SiO_2–Ag nanocomposites with enhanced visible-light photocatalytic activity, ACS Appl. Mater. Interfaces, 5 (2013) 3824-3832.

[36] N. Boonprakob, N. Wetchakun, S. Phanichphant, D. Waxler, P. Sherrell, A. Nattestad, J. Chen, B. Inceesungvorn, Enhanced visible-light photocatalytic activity of g-C_3N_4/TiO_2 films, J. Colloid Interface Sci., 417 (2014) 402-409.

[37] G.S. Wilson, Native glucose oxidase does not undergo direct electron transfer, Biosens. Bioelectron., 82 (2016) vii-viii.

[38] B. Liang, X. Guo, L. Fang, Y. Hu, G. Yang, Q. Zhu, J. Wei, X. Ye, Study of direct electron transfer and enzyme activity of glucose oxidase on graphene surface, Electrochem. Commun., 50 (2015) 1-5.

[39] M. Wooten, S. Karra, M. Zhang, W. Gorski, On the direct electron transfer, sensing, and enzyme activity in the glucose oxidase/carbon nanotubes system, Anal. Chem., 86 (2014) 752-757.

[40] J. Zhu, X. Huo, X. Liu, H. Ju, Gold nanoparticles deposited polyaniline–TiO_2 nanotube for surface plasmon resonance enhanced photoelectrochemical biosensing, ACS Appl. Mater.

Interfaces, 8 (2016) 341-349.

[41] S. Wu, H. Huang, M. Shang, C. Du, Y. Wu, W. Song, High visible light sensitive MoS_2 ultrathin nanosheets for photoelectrochemical biosensing, Biosens. Bioelectron., 92 (2017) 646-653.

[42] M. Zheng, Y. Cui, X. Li, S. Liu, Z. Tang, Photoelectrochemical sensing of glucose based on quantum dot and enzyme nanocomposites, J. Electroanal. Chem., 656 (2011) 167-173.

[43] X. Zhang, M. Liu, H. Liu, S. Zhang, Low-toxic Ag_2S quantum dots for photoelectrochemical detection glucose and cancer cells, Biosens. Bioelectron., 56 (2014) 307-312.

[44] L. Xu, J. Xia, L. Wang, J. Qian, H. Li, K. Wang, K. Sun, M. He, α-Fe_2O_3 cubes with high visible-light-activated photoelectrochemical activity towards glucose: hydrothermal synthesis assisted by a hydrophobic ionic liquid, Chem. - Eur. J., 20 (2014) 2244-2253.

[45] W. Wang, L. Bao, J. Lei, W. Tu, H. Ju, Visible light induced photoelectrochemical biosensing based on oxygen-sensitive quantum dots, Anal. Chim. Acta, 744 (2012) 33-38.

[46] X. Zhang, F. Xu, B. Zhao, X. Ji, Y. Yao, D. Wu, Z. Gao, K. Jiang, Synthesis of CdS quantum dots decorated graphene nanosheets and non-enzymatic photoelectrochemical detection of glucose, Electrochim. Acta, 133 (2014) 615-622.

[47] A.I. Gopalan, N. Muthuchamy, K.P. Lee, A novel bismuth oxychloride-graphene hybrid nanosheets based non-enzymatic photoelectrochemical glucose sensing platform for high performances, Biosens. Bioelectron., 89, Part 1 (2017) 352-360.

Figure Captions

Scheme 1. Schematic illustration for preparation of GOx|g-C_3N_4-TiO_2|ITO composite.

Scheme 2. Mechanism for PEC detection of glucose at GOx|g-C_3N_4-TiO_2|ITO.

Figure 1. (a) X-ray diffraction patterns of i TiO_2 nanosheets, ii g-C_3N_4 and iii g-C_3N_4-TiO_2 composite; (b) Fourier transform infrared spectra of (i) TiO_2 nanosheets, (ii) g-C_3N_4 and (iii) a g-C_3N_4-TiO_2 composite; (c) UV–Vis diffuse reflectance spectra of i g-C_3N_4, ii g-C_3N_4-TiO_2 and iii TiO_2 nanosheets.

Figure 2. Transmission electron micrographs of (a) g-C_3N_4, (b) and (c) g-C_3N_4-TiO_2 composite, (d) scanning electron micrograph of TiO_2 nanosheets.

Figure 3. (a) X-ray photoelectron survey spectrum of g-C_3N_4-TiO_2, the high resolution spectra of the (b) C1s, (c) N1s, (d) Ti2p and (e) O1s peaks from a g-C_3N_4-TiO_2 composite.

Figure 4. (a) Nyquist plots of 5.0 mM $[FeCN_6]^{3-}$ and 5.0 mM $[FeCN_6]^{4-}$ at (i) a bare ITO, (ii) a g-C_3N_4|ITO, (iii) a g-C_3N_4-TiO_2|ITO and (iv) a GOx|g-C_3N_4-TiO_2|ITO in 0.1 M KCl in air; Top left inset: cyclic voltammogram of 5.0 mM $[FeCN_6]^{3-}$ and 5.0 mM $[FeCN_6]^{4-}$ at a GOx|g-C_3N_4-TiO_2|ITO in 0.1 M KCl at a scan rate of $0.1Vs^{-1}$; bottom right inset: equivalent circuit and optimal values for the circuit elements used in the computer simulations of the experimental impedance plots; (b) Cyclic voltammetry at GOx|g-C_3N_4-TiO_2|ITO in (i) 0.1 M N_2-saturated PBS (pH 7.4), and in air-saturated PBS with (ii) 0 mM, (iii) 1 mM, (iv) 4 mM, and (v) 8 mM glucose at a scan rate of $0.1Vs^{-1}$; (c) The effect of Nafion concentration on the photocurrent response of GOx|g-C_3N_4-TiO_2|ITO in the presence of 1 mM glucose; (d) The effect of mass ratio between GOx and the composite on the photocurrent response of GOx|g-C_3N_4-TiO_2|ITO in the presence of 1 mM glucose.

Figure 5. (a) Photocurrent response of (i) TiO_2|ITO, (ii) g-C_3N_4|ITO, (iii) GOx|g-C_3N_4-TiO_2|ITO, (iv) g-C_3N_4-TiO_2|ITO, and (v) GOx|g-C_3N_4-TiO_2|ITO in the presence of

0.1 mM glucose in 0.1 M PBS pH 7.4 at an applied potential of 0.2 V; (b) Photocurrent response of the GOx|g-C_3N_4-TiO_2|ITO at an applied potential of 0.2 V with increasing concentrations of glucose (a-i): 0, 0.05, 0.1, 0.5, 2.0, 4.0, 8.0, 12 and 16 mM, respectively; (c) A photocurrent versus glucose concentration calibration plot based on results in (b); (d) Photocurrent response of GOx|g-C_3N_4-TiO_2|ITO in 0.1 M PBS (pH 7.4) containing 1 mM glucose and 0.1 mM other interferents: ascorbic acid (AA), uric acid (UA), dopamine (DA), fructose (Fruc), lactose (Lac) and sucrose (Suc).

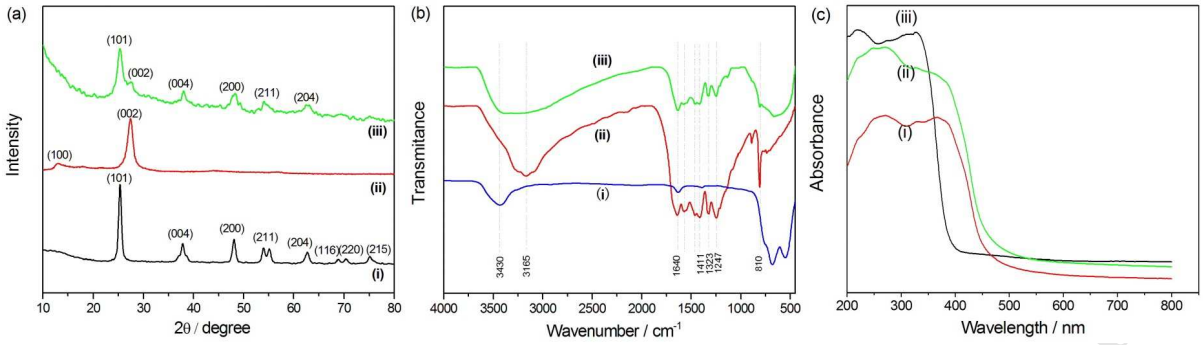

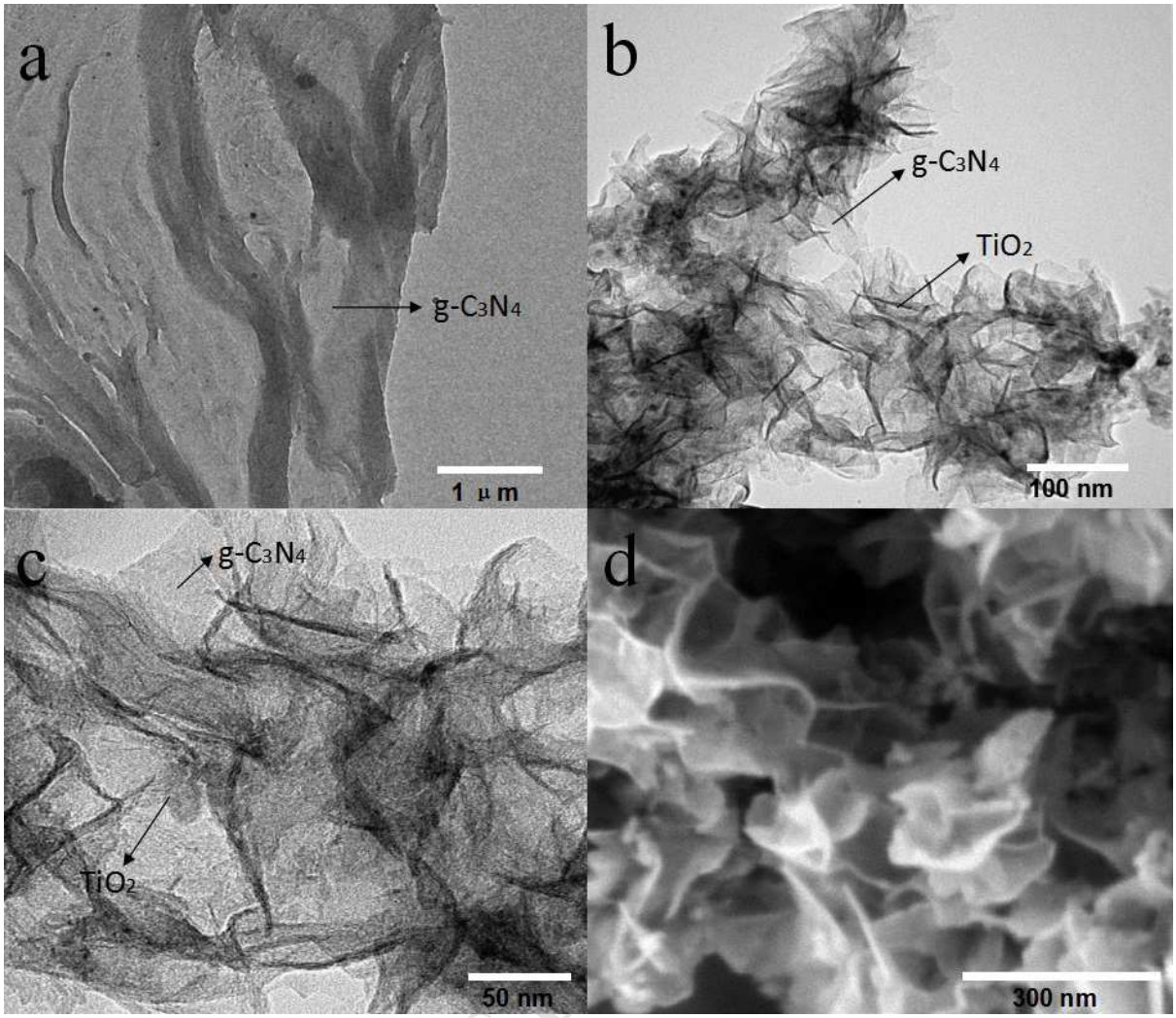

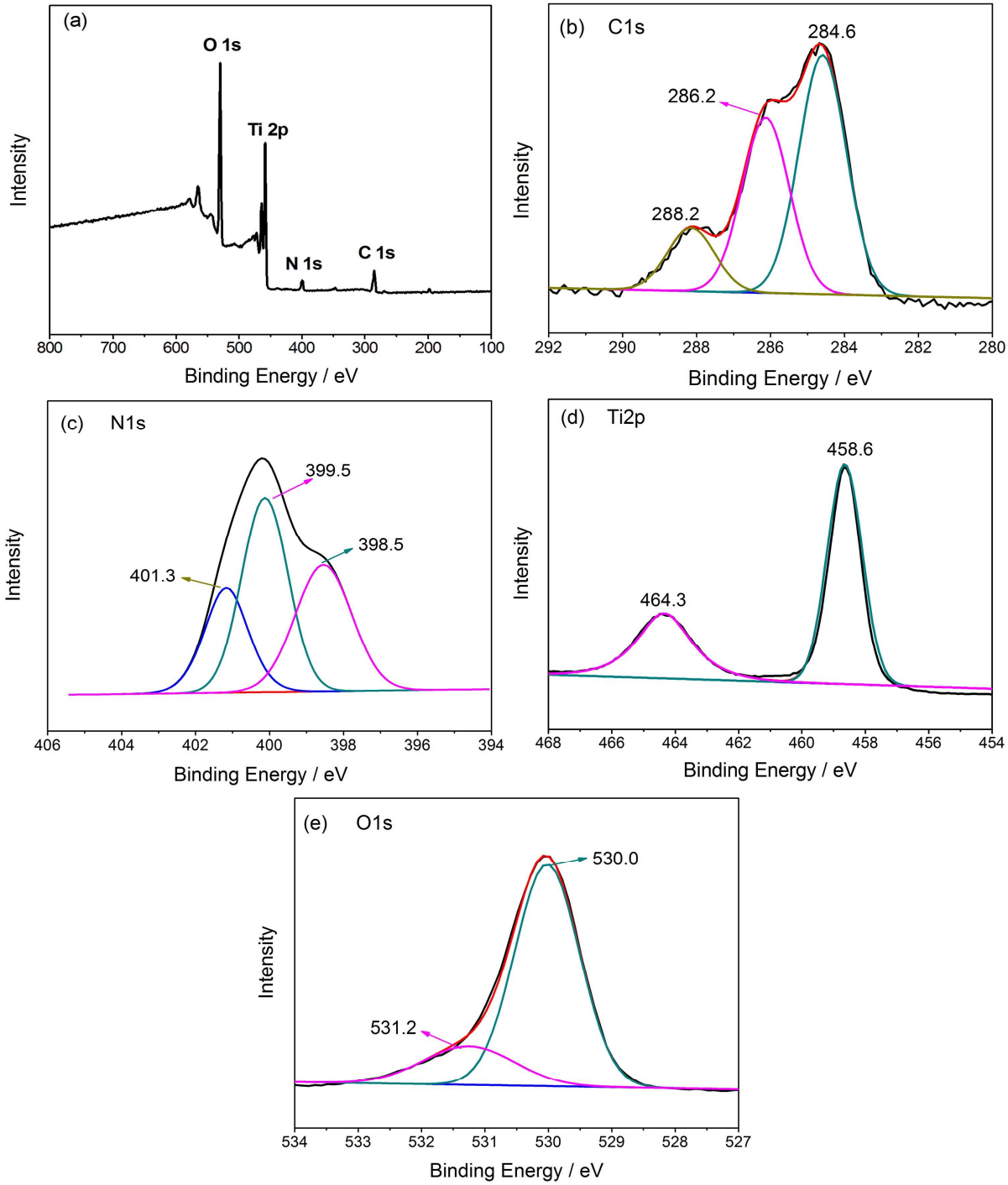
(a)
O 1s
Ti 2p
N 1s
C 1s
Intensity
800 700 600 500 400 300 200 100
Binding Energy / eV
(b) C1s
284.6
286.2
288.2
Intensity
292 290 288 286 284 282 280
Binding Energy / eV
(c) N1s
399.5
398.5
401.3
Intensity
406 404 402 400 398 396 394
Binding Energy / eV
(d) Ti2p
458.6
464.3
Intensity
468 466 464 462 460 458 456 454
Binding Energy / eV
(e) O1s
530.0
531.2
Intensity
534 533 532 531 530 529 528 527
Binding Energy / eV

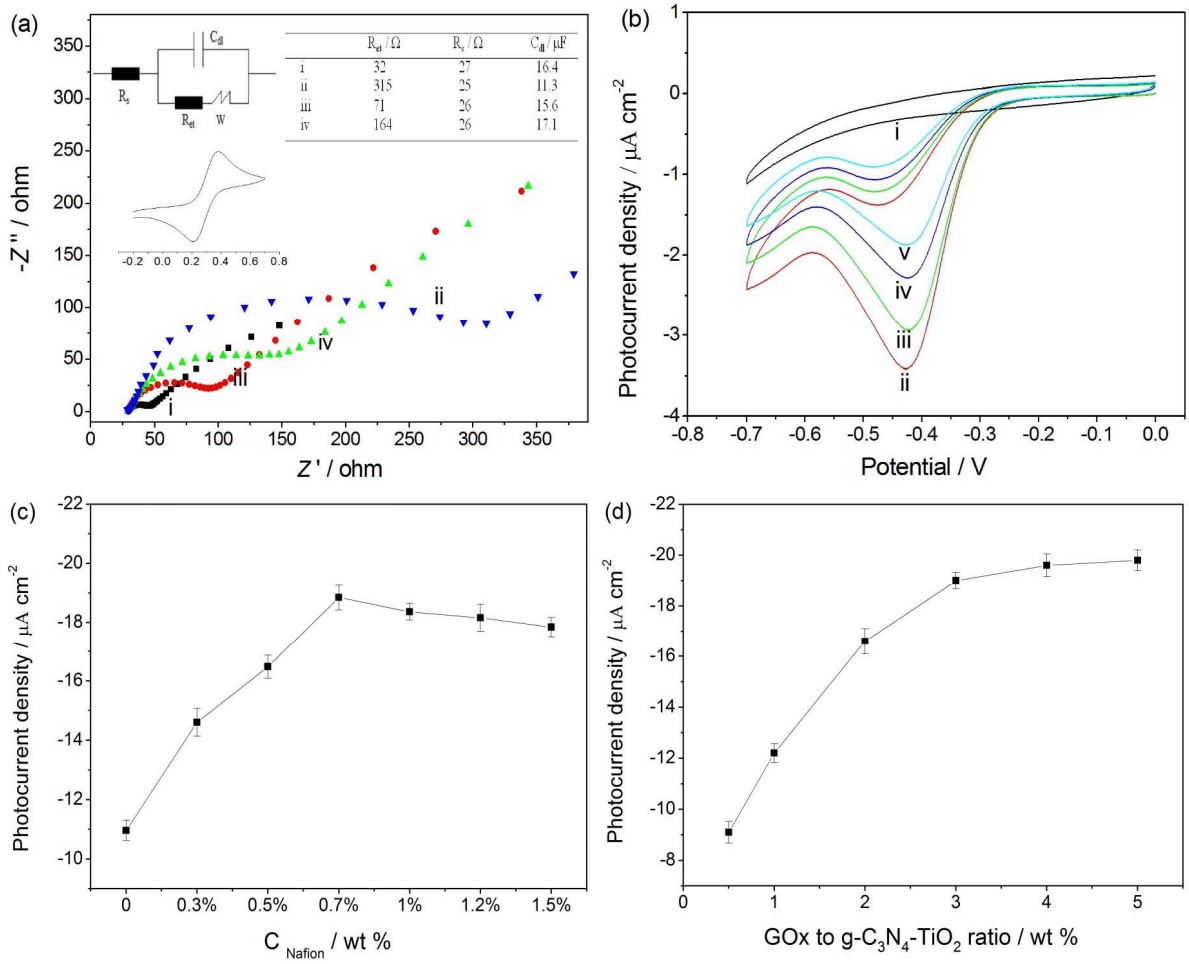
(a)
-Z'' / ohm
Z' / ohm
i
ii
iii
iv
C_{dl}
R_s
R_{et}
W
R_{et} / Ω
R_s / Ω
C_{dl} / μF
i 32 27 16.4
ii 315 25 11.3
iii 71 26 15.6
iv 164 26 17.1
(b)
Photocurrent density / μA cm^{-2}
Potential / V
i
ii
iii
iv
v
(c)
Photocurrent density / μA cm^{-2}
C_{Nafion} / wt %
(d)
Photocurrent density / μA cm^{-2}
GOx to g-C_3N_4-TiO_2 ratio / wt %

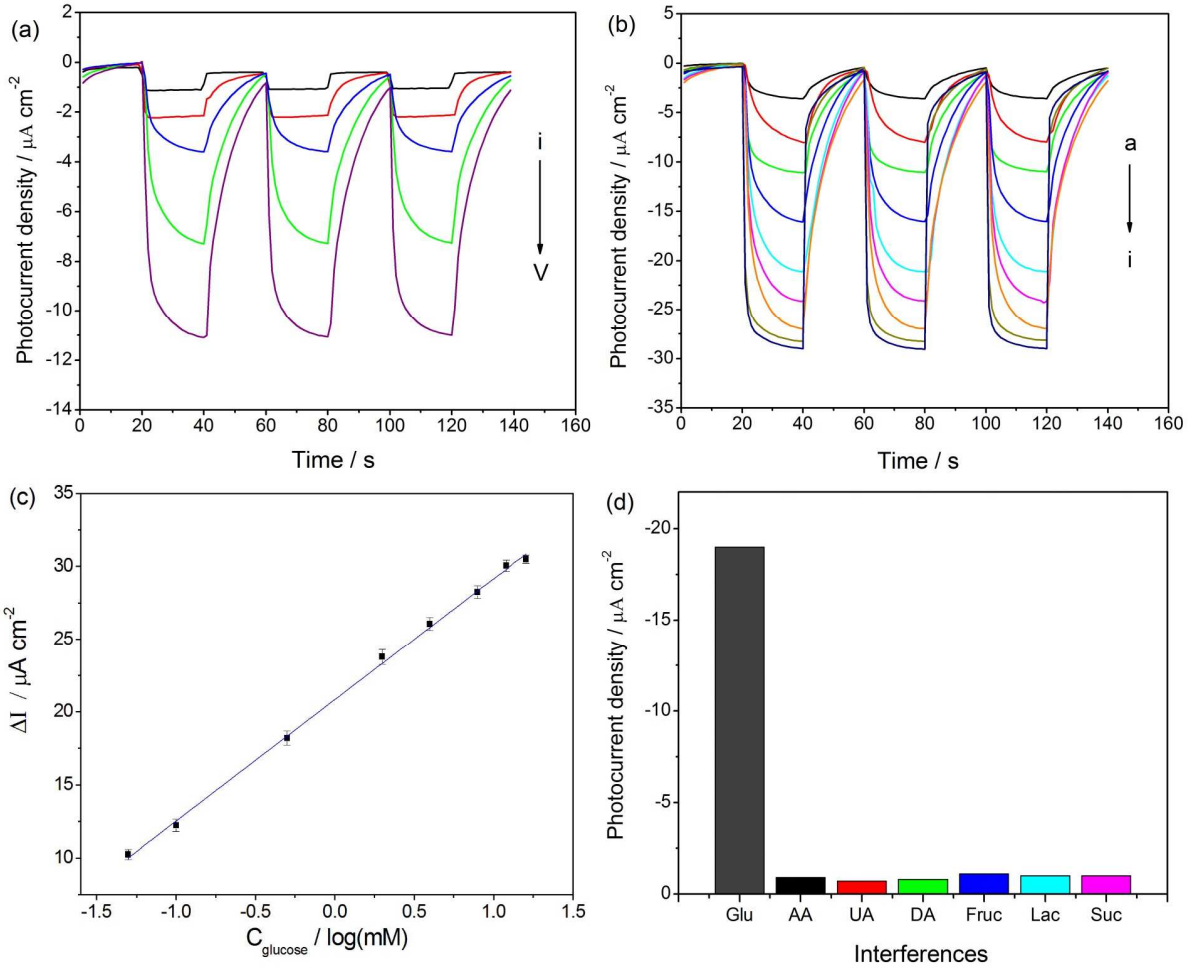
(a)
Photocurrent density / μA cm-2
Time / s
i
V
(b)
Photocurrent density / μA cm-2
Time / s
a
i
(c)
ΔI / μA cm-2
Cglucose / log(mM)
(d)
Photocurrent density / μA cm-2
Glu
AA
UA
DA
Fruc
Lac
Suc
Interferences

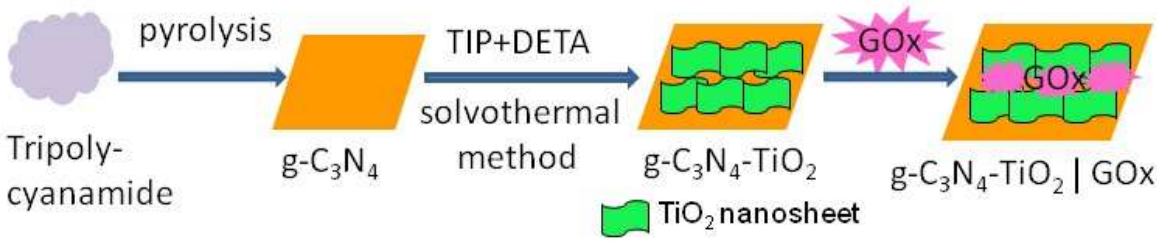

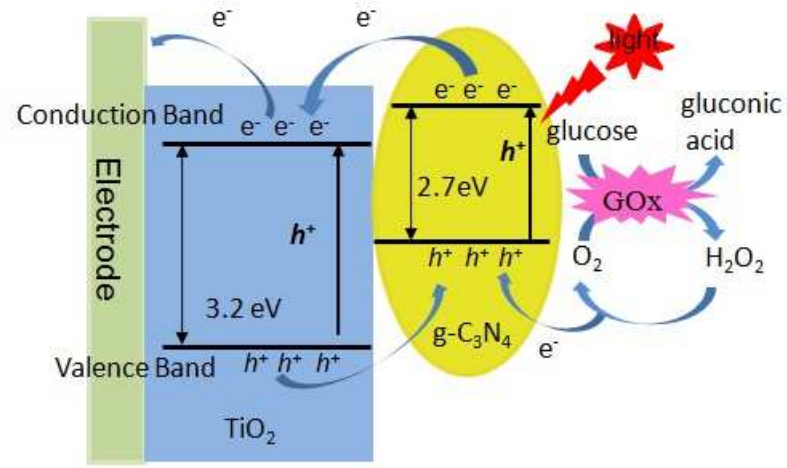

Highlights

- A photoelectrochemical enzyme biosensor
- A TiO_2 nanosheet-g-C_3N_4 composite as a biosensor scaffold
- A photoelectrochemical biosensor operable using visible excitation